Environmental Science and Pollution Research (2022) 29:75989–76002
https://doi.org/10.1007/s11356-022-20764-3

RESEARCH ARTICLE

Adsorption of Co(II) ions using Zr-Ca-Mg and Ti-Ca-Mg phosphates: adsorption modeling and mechanistic aspects

Andrei Ivanets[1] · Irina Shashkova[1] · Natalja Kitikova[1] · Natalia Drozdova[1] · Anastasiya Dzikaya[1] · Oleg Shichalin[2] · Sofiya Yarusova[3,4] · Evgeniy Papynov[2]

Received: 26 January 2022 / Accepted: 7 May 2022 / Published online: 4 June 2022

Abstract

The environmental pollution by toxic Co(II) ions had a negative impact on living organisms and water resources. The amorphous Zr-Ca-Mg and Ti-Ca-Mg phosphates with varied Zr and Ti content with the mesoporous structure (A_{BET} = 19–232 m^2/g, $V_{des.}$ = 0.075–0.370 cm^3/g, $D_{des.}$ = 6.2–10.9 nm) were synthesized. The effect of adsorbent chemical composition, the presence of competing ions (0.1–1.0 M NaCl and 0.01–0.1 M $CaCl_2$ backgrounds), and pH (3.0–7.0) of aqueous solution on adsorption removal of Co(II) ions by Zr-Ca-Mg and Ti-Ca-Mg phosphates was studied. The highest adsorption capacity of Zr-Ca-Mg-1 and Ti-Ca-Mg-1 samples reached 253.3 and 212.8 mg/g. The prepared adsorbents demonstrated high efficiency at pH in the range of 3.0–7.0 and the presence of 0.1–1.0 M NaCl and seawater with a salinity of 35.0 g/L backgrounds. The chemisorption and ion-exchange mechanisms of Co(II) ions removal for Zr-Ca-Mg and Ti-Ca-Mg phosphates were proposed. The adsorption isotherms were well fitted with Sips and Langmuir models that proved the heterogeneous nature of adsorption sites as well as assumed the monolayer adsorption that occurs at specific homogeneous sites within the adsorbent without any interaction between the adsorbed substances. The kinetic data was well described by the pseudo-second-order model that is suitable for chemisorption processes as liming adsorption stage. The presented results shown the prospects of developed adsorbents for the investigation of real wastewater treatment from heavy metal ions and liquid radioactive waste purification.

Keywords Zr-Ca-Mg phosphates · Ti-Ca-Mg phosphates · Co(II) ions adsorption · Isotherms and kinetic modeling · Water treatment

Introduction

The intensive growth and development of global industrial production are accompanied by the continuous search and development of more efficient materials and technologies to solve environmental problems related to the protection of soils, water basins, as well as humans themselves from the toxic effects of anthropogenic pollutants (Yarusova et al. 2015; Vareda et al. 2019; Carolin et al. 2017; Qasem et al. 2021; Mudhoo et al. 2021; Khalid et al. 2016; Prasad and Saxena 2004). Heavy metals, including Co(II) ions, are among the most common highly toxic and biodegradable pollutants that harm on living organisms due to ingress into water and soil and are capable of accumulating in the human body, leading to irreversible health consequences (Camara-Martos and Moreno-Rojas 2016; Hasan et al. 2017; Balzani et al. 2021). According to (Islam et al. 2018), the maximum permissible concentration (MPC) of Co(II) ions in drinking water should not exceed 0.05 mg/L (Mohod and Dhote 2013) .

Responsible Editor: Tito Roberto Cadaval Jr.

✉ Andrei Ivanets
ivanets@igic.bas-net.by; Andreiivanets@yandex.ru

[1] Institute of General and Inorganic Chemistry of the National Academy of Sciences of Belarus, Surganova St, 9/1, 220072 Minsk, Belarus

[2] Far Eastern Federal University, Russky Island, 10 Ajax Bay, 690922 Vladivostok, Russia

[3] Institute of Chemistry, Far Eastern Branch of Russian Academy of Sciences, 159, Prosp. 100-letiya Vladivostoka, Vladivostok 690022, Russia

[4] Vladivostok State University of Economics and Service, Gogolya St 41, 690014 Vladivostok, Russia

Cobalt is recognized by the European Commission as a "Critical Raw Material" due to its irreplaceable functionality in many types of modern technology, combined with its current high-risk status associated with its supply. Despite such importance, there remain major knowledge gaps with regard to the geochemistry, mineralogy, and microbiology of cobalt-bearing environments, particularly those associated with ore deposits and subsequent mining operations. In such environments, high concentrations of Co(II) (up to 34.400 mg/L in mine water, 14.165 mg/kg in tailings, 21.134 mg/kg in soils, and 18.434 mg/kg in stream sediments) have been documented (Ziwa et al. 2021).

Cobalt compounds are widely used in metallurgical processes, are part of lithium-ion batteries and metal oxide catalysts, which leads to an increased content in industrial wastewater, and are also often found in groundwater (Wu et al. 2015; Islam et al. 2018). In addition, long-lived radioisotopes ^{60}Co and ^{58}Co are an invariable component of liquid radioactive waste from nuclear power plants and radiation medicine (Kobayashi and Suzuki 2013).

Various methods are used for metal ions removal from aqueous solutions: chemical precipitation (Chen et al. 2018), ion exchange, adsorption (Singh et al. 2018; Mudhoo et al. 2021; Joseph et al. 2019), membrane filtration (El Batouti et al. 2021), reverse osmosis, electrochemical methods (Ghernaout and Elboughdiri 2020), extraction (Qasem et al. 2021), and biological treatment (Hasan et al. 2020). However, the adsorption method is mainly being investigated for the Co(II) ions removal. An important feature of Co(II) ions is their high susceptibility to hydrolysis and polymerization in aqueous solutions, the formation of strong complexes with natural humic and fulvic acids. At the same time, depending on the concentration of Co(II) ions and the pH of the medium, hydrated Co^{2+} ions, mono- and polynuclear hydroxo complexes of various compositions, colloidal particles of cobalt hydroxide are present in solutions (Kishi et al., 1998). It has a significant impact on the effectiveness of the methods used for wastewater and natural water treatment. In connection with the above, the removal of Co(II) ions from aqueous solutions is a complex problem.

Natural and synthetic adsorbents (Islam et al. 2018; Singh et al. 2018; Mudhoo et al. 2021; Joseph et al. 2019; Khalid et al. 2016) are widely used for the removal of heavy metal ions from aqueous media and soil remediation. A special position among inorganic adsorbents is occupied by hardly soluble phosphates of two- and four-valent metals. Thus, calcium-magnesium phosphates (Lyczko et al. 2014; Ivanets et al. 2017; Ivanets et al. 2019a, b) and zirconium and titanium phosphates (Veliscek-Carolan et al. 2017; Pan et al. 2022; Pica 2021; Maslova et al. 2020; Maslova et al. 2021) are characterized by an increased affinity for a large number of polyvalent metal ions (Pb^{2+}, Cd^{2+}, Co^{2+}, Zn^{2+}, Cu^{2+}, Cs^{+}, Sr^{2+} etc.) and exhibit a wide variety of adsorption mechanisms. During the adsorption of 3d-metal cations, less soluble phosphate compounds are formed. The bond strength of the adsorbed cation with the adsorbent is the most important characteristic for their practical application since 3d-metal ions have low MPC, and even small desorption from the surface of the adsorbent can lead to secondary contamination.

One of the directions of developing more efficient materials and technologies for extracting heavy metals from solutions is developing research in the field of synthesis of composite adsorption materials, including phosphate. Composite materials, as a rule, consist of two or more components with different physical and chemical properties, due to which the composite material surpasses the individual components of the composite in specific properties and has a wider range of properties and applications (Ekka et al. 2018; Ali et al. 2019; Butt et al. 2020).

Previously, we developed simple methods for the synthesis of composite adsorbents based on Zr-Ca-Mg and Ti-Ca-Mg phosphates from widely available and widespread natural raw materials of dolomite (Ivanets et al. 2019b, 2021; Maslova et al. 2020). Their high efficiency in the adsorption of long-lived ^{90}Sr, ^{137}Cs, ^{60}Co radionuclides from model solutions of complex composition, which determine the main dose load of liquid radioactive waste, was shown. Herewith, composite phosphates are superior in efficiency to individual calcium-magnesium phosphates and individual zirconium and titanium phosphates. In addition, individual phosphates cannot adsorb all three radionuclides, which makes it possible to expand the scope of these adsorbents.

It is important to note that the behavior of inorganic adsorbents significantly depends on many factors, including the concentration of toxic cations, the presence of competing cations, salinity, and pH. It was shown that the effectiveness of adsorbents based on Ti-Ca-Mg phosphates differs in the removal of stable metal ions and radionuclides, due to the low concentrations of the radioactive isotopes (10^{-7}–10^{-9} mol/L) (Ivanets et al. 2020).

The purpose of this work was to study the adsorption properties of composite Zr-Ca-Mg and Ti-Ca-Mg phosphates of various compositions to Co(II) ions and to establish a relationship between synthesis–structure–adsorption properties. The novelty of the work devoted to the firstly investigation of adsorption modeling and mechanistic aspects of prepared Ti-Ca-Mg and Zr-Ca-Mg phosphates to Co(II) ions. The further application of prepared adsorbents for liquid radioactive waste treatment and ^{60}Co radionuclide immobilization were specific objectives. The main tasks include (i) the influence of the nature and concentration of competing cations, as well as the pH of aqueous solutions on the adsorption efficiency of Co(II) ions; (ii) the different mechanisms of Co(II) ions removal for Zr-Ca-Mg and Ti-Ca-Mg phosphates depend on Zr and Ti content in

composites were proposed; and (iii) the isotherms and kinetics modeling were performed. The obtained results are of key importance for the practical application of the obtained adsorbents and optimization of adsorption technologies.

Materials and methods

Cost effectiveness is the chief factor for development of any adsorbent and its successful industrial application.

Thus, the starting material for the synthesis of mixed Zr-Ca-Mg and Ti-Ca-Mg phosphates was thermally activated dolomite at 800 °C (Ruba deposit, Belarus) with a Ca and Mg content of 6.74 and 6.55 mmol/g. Phosphoric acid H_3PO_4 (85 wt. %) and zirconyl nitrate $ZrO(NO_3)_2$ for synthesis, $Co(NO_3)_2{\cdot}6H_2O$, NaCl, and $CaCl_2$ for adsorption study were of analytical grade and used without further purification. Titanium salt with $(NH_4)_2TiO(SO_4)_2{\cdot}H_2O$ formula (ammonium titanyl sulfate) was used as a titanium precursor. This salt has been obtained from industrial waste of apatite-nepheline ore processing (Maslova et al. 2020).

Synthesis of composite Zr-Ca-Mg and Ti-Ca-Mg phosphates

At the first stage, phosphating of calcined dolomite was carried out at an *m/V* ratio equal to 1:3, where *m* is the weight of thermally activated dolomite (g) and *V* is the volume (mL) of 20 wt.% phosphoric acid solutions. Under these conditions, phosphatized dolomite of the $Ca_{0.7}Mg_{0.3}HPO_4{\bullet}2H_2O$ composition was obtained, which was a mixture of amorphous calcium and magnesium hydrogen phosphates (Ivanets et al. 2017).

The synthesis of mixed Ti-Ca-Mg phosphates was carried out by reacting phosphatized dolomite with a 3.85% aqueous solution of titanyl diammonium sulfate $(NH_4)_2TiO(SO_4)_2{\cdot}H_2O$ at a *V/m* ratio of 60/4 ml/g (sample Ti-Ca-Mg-1 or abbreviated Ti-1) and 180/4 ml/g (sample Ti-Ca-Mg-2 or Ti-2) at a temperature of 25 °C.

Mixed Zr-Ca-Mg phosphates containing 2.2 (sample Zr-Ca-Mg-1 or abbreviated Zr-1) and 6.6 mmol Zr/g (sample Zr-Ca-Mg-2 or Zr-2) of phosphatized dolomite were obtained by reacting phosphatized dolomite with a 2 wt.% aqueous solution of zirconyl nitrate $ZrO(NO_3)_2$.

Adsorbents characterization

Data on the phase composition of the initial and spent adsorbents were obtained using X-ray phase analysis (XRD) performed on an X-ray diffractometer D8 Advanced (Bruker, Germany) using CuKα radiation at 2Θ range 5−60°. The chemical composition of samples was identified by the energy-dispersive X-ray spectroscopy with AZtecLive Advanced with Ultim Max 40 detector (Oxford Instruments, Bognor Regis, UK).

The adsorption properties and texture of the samples were evaluated from isotherms of low-temperature (− 196 °C) physical adsorption–desorption of nitrogen measured by the volumetric method on the ASAP 2020 MP surface area and porosity analyzer (Micromeritics, USA). The specific surface area was calculated by the BET method (A_{BET}); the pore volume was calculated by a single-point method using the desorption ($V_{sp.\ des.}$) isotherm branch. According to the obtained data, the average pore diameter for the desorption isotherm branch ($D_{sp.\ des.}$) was calculated according to Eq. 4 V/A. Before analysis, the samples were evacuated for 1 h at a temperature of 150 °C and a residual pressure of 133.3×10^{-3} Pa. The relative error in determining the pore volume was ± 1%, the surface area, and pore size of ± 15%.

To interpret the dependence of the adsorption properties of composite phosphates on pH, the adsorbents pH zero point charge (pH_{zpc}) was determined. The experiment was carried out by pH measuring of solutions after contact of 0.040 g of adsorbent with 10.0 mL of 0.01 M NaCl solution (V/m 250 mL/g), the pH of which varied from 3.0 to 12.0. The suspension was kept for 24 h with constant stirring on an orbital shaker at a rate of 200 rpm. The adsorbent was separated from the filtrate by filtering through a paper filter "white tape." Furthermore, the equilibrium pH of the solution was measured, and pH_{zpc} was determined graphically (Nasiruddin and Server, 2007).

Adsorption experiment

Effect of adsorption conditions

Adsorption of Co(II) ions was carried out under static conditions from aqueous nitrate solutions $Co(NO_3)_2{\cdot}6H_2O$ in the concentration range of 50–2500 mg/L to study the adsorption isotherms and 500 mg/L for kinetic studies. The maximum capacity of adsorbents was determined from 0.05 M $Co(NO_3)_2{\cdot}6H_2O$ solutions. Sample of 0.1 g adsorbent was mixed with 25 mL of aqueous Co(II) solutions (dose of 4.0 g/L) at periodical mixing. The study of adsorption kinetics was carried out with a contact time from 10 min to 24 h. For other experiments, the contact time was 24 h. The pH of solutions was adjusted with 0.5 M HNO_3 and NaOH solutions during the study of the effect of pH in the range of 3.0−7.0 on the adsorption capacity. The effect of electrolyte on Co(II) adsorption efficiency was studied at 1000 mg/L with NaCl (0.1 and 1.0 mol/L) or $CaCl_2$ (0.01 and 0.1 mol/L) backgrounds. After experiment, adsorbents were filtered using paper filter "blue ribbon," washed by distillated water, and dried at 65 °C. The Co(II) ions concentration in the initial and purified solutions was determined

by atomic absorption spectroscopy on the SpectrAA 220FS atomic absorption spectrometer.

Isotherms modeling

The adsorption capacity q (mg/g), removal efficiency α (%), and the rate of adsorption equilibrium reaching F were calculated using the appropriate Eqs. (1–3):

$$\alpha = \frac{C_0 - C}{m} \times V \tag{1}$$

$$\alpha = \frac{C_0 - C}{C_0} \times 100 \tag{2}$$

$$F = \frac{q_t}{q_e} \tag{3}$$

where C_0 and C (mg/l) are the initial and residual concentrations of metal ions in the filtrate after adsorption, V (L) is aliquot volume, m (g) is adsorbent weight, and q_t and q_e (mg/g) are adsorption capacity at time t and after equilibrium reaching.

Well-known mathematical models Eqs. (4–9) were used to describe the obtained isotherms. In addition, their modifications Eqs. (5, 8, 11) were applied, taking into account the features of experimental curves, in particular, having a sigmoid (S-shaped) shape (Limousin et al. 2007; Wang and Guo 2020):

Langmuir equation:

$$q_e = \frac{q_m K_L C_e}{1 + K_L C_e} \tag{4}$$

$$q_e = \frac{q_m K_L C_e}{1 + K_L C_e + S/C_e} \tag{5}$$

where q_m and q_e (mg/g) are maximum and equilibrium adsorption capacity, C_e (mg/L) is equilibrium concentration of Co(II) ions, K_L (L/mg) the coefficient of adsorption equilibrium characterizing the affinity of the adsorbate to the adsorbent, and S (mg/L) is the constant associated with the restriction of adsorption at low concentration (Limousin et al. 2007);

Freundlich equation:

$$q_e = K_F C_e^{1/n} \tag{6}$$

where K_F ((mg/g)/(L/mg)^n_F) and n_F are the adsorption constants of Freundlich related to the adsorption capacity and the affinity of the adsorbent, respectively;

– Sips equation (Eq. 7) and Redlich-Peterson equation (Eq. 9) are hybrid models combining the Langmuir and Freundlich equations (Wang and Guo, 2020):

$$q_e = \frac{q_m K_S C_e^{n_s}}{1 + K_S C_e^{n_s}} \tag{7}$$

where K_S (L/mg) is a constant reflecting the affinity of the adsorbate to the adsorbent, n_S is a constant describing the surface homogeneity. For the sigmoid isotherm form, this equation takes the following form:

$$q_e = \frac{q_m K_S C_e^{n_s}}{1 + K_S S/C_e} \tag{8}$$

– Redlich-Peterson equation:

$$q_e = \frac{K_{RP} C_e}{1 + a_{RP} C_e^g} \tag{9}$$

where K_{RP} (L/g) and a_{RP} (L^g/mg^g) are Redlich-Peterson constants; g is the exponent whose values should fit into the interval $0 < g \leq 1$. For $g = 1$, the model reduces to the Langmuir equation. This equation can be represented in a different form (Eq. 10), preserving the symbols of the parameters (Eq. 9) (Wu et al. 2010):

$$q_e = \frac{q_m a_{RP} C_e}{1 + a_{RP} C_e^g} \tag{10}$$

then $K_{RP} = q_e \cdot a_{RP}$, and $q_m = K_{RP}/a_{RP}$.

To characterize the correspondence of the obtained experimental data to the adsorption models, the approximation coefficient R^2, sum of the squares of the errors (SSE), and standard error (SE) were calculated:

$$R^2 = \frac{\sum \left(q_{e,exp} - \overline{q}_{e,exp}\right)^2 - \sum \left(q_{e,exp} - \overline{q}_{e,calc}\right)^2}{\sum \left(q_{e,exp} - \overline{q}_{e,exp}\right)^2} \tag{11}$$

$$SSE = \sum \left(q_{e,exp} - \overline{q}_{e,calc}\right)^2 \tag{12}$$

$$SE = \sqrt{\frac{1}{m-p} \sum \left(q_{e,exp} - \overline{q}_{e,exp}\right)^2} \tag{13}$$

where $q_{e,calc}$ is the equilibrium capacity calculated from the isotherm equation, $q_{e,exp}$ is the equilibrium capacity obtained experimentally, $\overline{q}_{e,exp}$ is average value $q_{e,exp}$, m is a number of experimental points, and p is a number of parameters of the isotherm model.

Processing of experimental data for compliance with the presented models was carried out using the Microsoft Excel spreadsheet editor by searching for parameter values that

provide minimum error values of *SSE* and *SE*, as well as maximum values of R^2.

Kinetics modeling

The study of adsorption kinetics was carried out under similar conditions with a contact time from 10 min to 24 h. Mathematical processing of experimental kinetic data was carried out using the following models:

- pseudo-first-order (Lagergren):

$$ln\left(q_e - q_t\right) = lnq_e - k_1 t \tag{14}$$

- pseudo-second-order (Ho and McKay):

$$\frac{t}{q_t} = 1/\left(k_2 {q_e}^2\right) + \left(1/q_e\right)t, \tag{15}$$

- intraparticle diffusion (Weber and Morris):

$$q_t = {k_{int}}^{1/2} + C_{int} \tag{16}$$

where q_e and q_t (mg/g) are equilibrium and at time t adsorption capacity, k_1, (1/min), k_2, (g/(mg•min)), and k_{int} (mg/(g•min$^{0.5}$) are constant rate; $h = k_2 {q_e}^2$ (mg/(g•min)) is the initial adsorption rate, C_{int} is coefficient characterizing the diffusion layer, and B_{id} (mg/g) is constant associated with the thickness of the boundary layer (Lima et al. 2015).

Results and discussions

Chemical composition, texture, and surface properties.

The chemical composition, textural properties, and pH of the zero point charge of phosphates used in adsorption studies are presented in Table 1. According to EDX analysis, the synthesized Ti(Zr)-Ca-Mg composite phosphates had different chemical compositions (Table 1), due to different synthesis conditions. An increase in the concentration of precursors of salts of tetravalent metals led to a decrease in the content of calcium and magnesium in the samples due to their replacement with zirconium and titanium, which caused a corresponding increase in their content in the studied samples. According to the XRD data (Fig. 1), mixed Ti(Zr)-Ca-Mg-1 phosphates with a lower M(IV) content were composites containing amorphous zirconium or titanium phosphate and calcium and magnesium hydrogen phosphates. Samples with the highest content of titanium and zirconium Ti(Zr)-Ca-Mg-2 were represented only by the amorphous phase.

The synthesized mixed phosphates were mesoporous materials that differ significantly depending on the composition in their textural characteristics—the specific surface

Table 1 Characteristics of composite Ti-Ca-Mg и Zr-Ca-Mg phosphates

Samples	Elemental composition (EDX data), at. %					Texture properties			pH_{zpc}
	Ca	Mg	Zr(Ti)	P	O	A_{BET}, m^2/g	$V_{des.}$, cm^3/g	$D_{des.}$, nm	
Ti-Ca-Mg-1	4.32	1.76	16.9	8.21	67.06	19	0.075	10.9	7.0
Ti-Ca-Mg-2	1.33	0.06	23.6	6.89	66.05	232	0.370	6.2	4.8
Zr-Ca-Mg-1	6.00	2.50	7.8	12.90	70.80	80	0.166	7.6	7.2
Zr-Ca-Mg-2	0.70	0.40	15.1	12.70	71.10	29	0.082	9.3	5.2

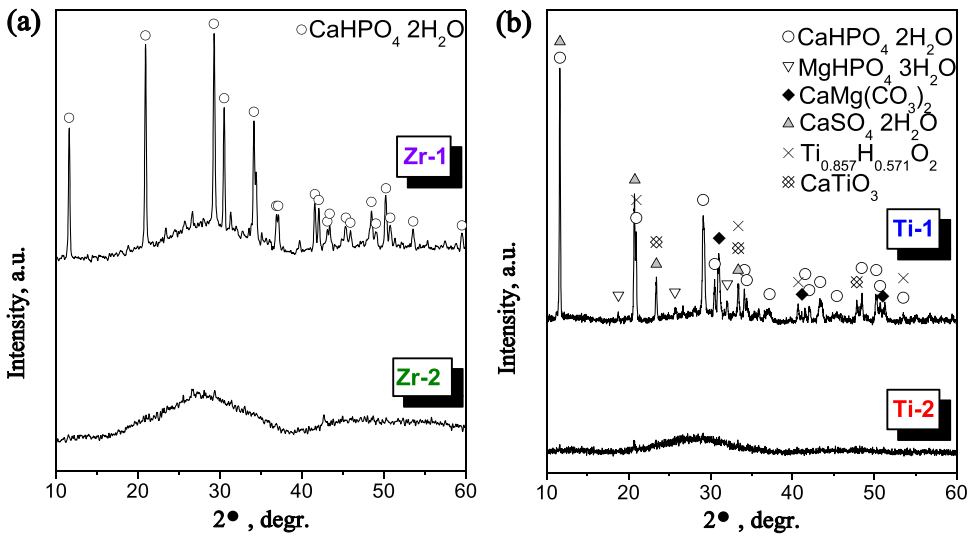

Fig. 1 XRD patterns of a Zr-Ca-Mg and b Ti-Ca-Mg phosphate adsorbents

area from 19 to 230 m^2/g, pore volume—0.075–0.370 cm^3/g, with an average pore diameter of 6.2–10.9 nm. The hysteresis loop in adsorption–desorption isotherms devoted to "bottle-like" and plate-like porous for Ti(Zr)-Ca-Mg-1 and Ti(Zr)-Ca-Mg-2 samples, respectively. The pore size distribution for Ti(Zr)-Ca-Mg-2 was narrow, when for Ti(Zr)-Ca-Mg-1 there was no pronounced maximum. At the same time, the pH_{zpc} for Zr- and Ti-containing samples had similar values and were 7.0–7.2 and 4.8–5.2 for Ti(Zr)-Ca-Mg-1 and Ti(Zr)-Ca-Mg-2, respectively.

Optimization of adsorption conditions

The adsorption capacity of adsorbents depends on many different factors (concentration of the adsorbed component, pH, and chemical composition of the solution, etc.). To determine the maximum sorption capacity of Co(II) ions, adsorption from 0.05 M (2950 mg/L) Co(II) solution was carried out. The adsorption capacity of Zr-Ca-Mg-1 and Ti-Ca-Mg-1 phosphates in highly concentrated 0.05 M cobalt nitrate solution reached 253.3 and 212.8 mg/g. Samples of Zr-Ca-Mg-2 and Ti-Ca-Mg-2 with a higher content of zirconium and titanium were adsorbed to 156.3 and 138.3 mg/g (Table 2).

To determine the effect of pH and electrolyte composition of the solution, the capacity of composite Zr-Ca-Mg and Ti-Ca-Mg phosphates from solutions with an initial concentration of Co(II) 1000 mg/L in the pH range 3.0–7.0 was determined. In the studied interval, the capacity of adsorbents varied depending on the composition of the phosphate adsorbents. Thus, the Zr-Ca-Mg-1 sample showed the highest efficiency in a slightly acidic and neutral medium (pH 5.0–7.0),

Table 2 The adsorption capacity of Co(II) ions of Zr-Ca-Mg and Ti-Ca-Mg phosphate

Solution	Adsorption capacity, q_e, mg/g			
	Zr-Ca-Mg-1	Zr-Ca-Mg-2	Ti-Ca-Mg-1	Ti-Ca-Mg-2
C_0 = 1000 mg/L				
pH 3.0	99.3	36.5	50.5	14.0
pH 5.0	109.8	38.8	39.0	15.0
pH 7.0	112.8	56.0	30.0	4.0
0.1 M NaCl	113.3	33.5	71.5	9.0
1.0 M NaCl	111.8	33.0	57.0	10.4
0.01 M $CaCl_2$	96.0	29.0	38.0	9.5
0.1 M $CaCl_2$	15.5	20.0	11.0	2.2
Seawater	130.1	13.1	129.2	12.9
C_0 = 2950 mg/L (0.05 M)				
Distilled water	253.3	156.3	212.8	138.3

while a decrease in pH to 3.0 was accompanied by a slight decrease in adsorption capacity from 110 to 99.3 mg/g. For the Zr-containing adsorbent Zr-Ca-Mg-2, a decrease in pH also negatively affected the adsorption capacity, while a decrease in the efficiency of the adsorbent was observed at pH 5.0 or less. The observed decrease in adsorption with acidification of the solution was following the Eqs. (17–19) of the heterogeneous reaction and ion exchange adsorption (acidification of the solution contributes to the shift of the equilibrium of these reactions to the left), as well as with the value of the pH_{zpc}. Herewith, in a more acidic solution, the dissolution of Ca and Mg hydrogen phosphates should increase, and accordingly the processes of precipitation of cobalt phosphate should increase. The presented results are well correlated with proposed mechanism of uptake from aqueous solution of divalent metal cations (Pb^{2+}, Cu^{2+}, and Zn^{2+}) by a low-cost mineral adsorbent (Prasad and Saxena, 2004).

$$2MgHPO_4 3H_2O + 3Co^2 + +2H_2O \rightarrow Co_3(PO_4)_2 8H_2O + 2Mg^2 + +2H^+ \quad (17)$$

$$2CaHPO_4 2H_2O + 3Co^2 + +2H_2O \rightarrow Co_3(PO_4)_2 8H_2O + 2Ca^2 + +2H^+ \quad (18)$$

$$Zr\left(HPO_4\right)_2 H_2OCo^{2+} \rightarrow ZrCo\left(PO_4\right)_2 H_2O + 2H^{2+} \quad (19)$$

For Ti-containing samples, an inverse relationship was observed—an increase in pH was accompanied by a decrease in the adsorption capacity of composite phosphates. At the same time, a noticeable decrease in the effectiveness of the Ti-Ca-Mg-1 and Ti-Ca-Mg-2 adsorbents occurred at pH 5.0 and 7.0, respectively. It is in a good agreement with values of pH_{zpc} and indicates differences between zirconium and titanium adsorbents. Thus, group IV elements differ greatly in their hydrolytic properties (Brown and Ekberg, 2016); in particular, Ge(IV) and Ti(IV) have acidic properties that predominate over the main ones, while Zr(IV) and Hf(IV) have the opposite. At $pH < pH_{zpc}$, the adsorbent surface is positively charged, which did not contribute to the adsorption of positively charged Co^{2+} ions. For Ti(Zr)-Ca-Mg-1 adsorbents, the best conditions were pH > 5.1, and for Ti(Zr)-Ca-Mg-2 pH > 7.1. The obtained data on the dependence of the adsorption properties of zirconium and titanium adsorbents on pH indicated a complex dependence of the effectiveness of the studied adsorbents on many factors: (i) hydrolytic properties of adsorbents, (ii) pH_{zpc}, (iii) the contribution of ion exchange and chemical interaction in adsorption depending on the composition of Zr-Ca-Mg and Ti Ca-Mg phosphates, (iv) the forms of Co(II) ions in solutions with different pH, etc.

The effect of competing cations on the adsorption efficiency of Co(II) ions was studied in solutions of NaCl (0.1 and 1.0 M), $CaCl_2$ (0.01 and 0.1 M) electrolytes, and from a model seawater solution with a total salinity of 35.0 g/L.

The presence of NaCl in the solution up to a concentration of 1.0 M did not significantly affect the capacity of the composite Zr-Ca-Mg and Ti-Ca-Mg sorbents. In the presence of a background electrolyte of 0.01 M $CaCl_2$, the adsorption capacity of all studied sorbents decreased slightly. The increase of $CaCl_2$ concentration up to 0.1 M led to a decrease in the adsorption capacity to 6.4–20.0 mg/g, which was 2–7 times less than for aqueous solutions without background electrolytes (Table 2).

It should be noted that in model solutions of seawater, there was an increase in the adsorption capacity for Zr-Ca-Mg-1 and Ti-Ca-Mg-1 samples and a decrease in the adsorption capacity of composite Zr-Ca-Mg-2 and Ti-Ca-Mg-2phosphates. This was because the main contribution to Co(II) adsorption for Zr-Ca-Mg-1 and Ti-Ca-Mg-1 interacted by calcium and magnesium hydrogen phosphates, which did not interact with NaCl and $CaCl_2$ and therefore retain selective properties in salt solutions to cobalt ions. Adsorbents with pronounced ion-exchange properties Zr-Ca-Mg-2 and Ti-Ca-Mg-2 did not exhibit selective properties in salt solutions.

Isotherms and mechanism studies

Experimental isotherms of Co(II) ions adsorption by composite phosphates from solutions of various concentrations, as well as isotherms calculated using various mathematical models, are shown in Fig. 2. The isotherms for Ti-Ca-Mg-1 Ti-Ca-Mg-2 adsorbents according to the Giles classification corresponded to the L-type, which characterizes the gradual saturation of the solid phase with adsorbate (Fig. 2a). Herewith, the adsorption isotherms for the Zr-Ca-Mg-1 and Zr-Ca-Mg-2 samples can be attributed to the H-type, which is a special case of the L-type isotherm and is characterized by a very high slope of the curve at the initial section of the isotherm at low concentrations (Fig. 2b). This course of the isotherm reflects the high affinity of adsorbents to Co(II) ions. A feature of the adsorption isotherms by Ti-containing samples was the absence of a plateau, which indicates the continued saturation of adsorbents with an increase in the concentration of the solutions.

The calculated parameters of the adsorption models used are presented in Table 3. Thus, the adsorption isotherms of cobalt ions strongly depended on the adsorbent chemical composition. The Co(II) ions ad on Zr-Ca-Mg-1 was described with a high degree of confidence by the Sips equation, and the values of the approximation coefficient had the highest value (R^2 0.991). In the case of other adsorbents, none of the applied equations gave high values of the approximation coefficient.

The highest values were obtained for Zr-Ca-Mg-2 also for the Sips equation (R^2 0.932). For Ti-Ca-Mg-1, all models except the Freundlich equation were applicable with the same degree of confidence (R^2 0.962), and for Ti-Ca-Mg-2, the best result was obtained for the Freundlich model. The higher values of the approximation coefficient R^2 for all adsorbents except Ti-Ca-Mg-2 obtained, using the hybrid Sips equation and the higher coincidence of the experimental adsorption capacity and calculated, allow us to conclude that the adsorption of Co(II) ions was heterogeneous at the initial site, and at high values of the equilibrium concentration of cobalt ions—monomolecular. For Ti-Ca-Mg-2, the maximum value of R^2 was obtained by applying the Freundlich equation, which indicated polymolecular heterogeneous adsorption.

The smallest calculated *SSE* and *SE* values in all cases except Ti-Ca-Mg-2 were obtained using the Sips equation.

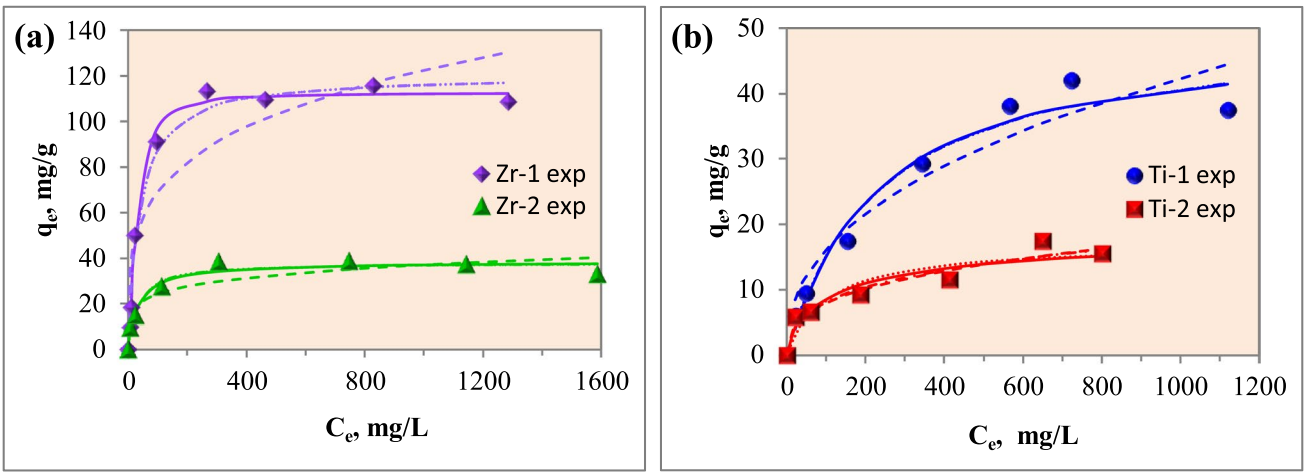

Fig. 2 Adsorption isotherms of Co(II) ions for **a** Zr-Ca-Mg-1 and Zr-Ca-Mg-2 and **b** Ti-Ca-Mg-1 and Ti-Ca-Mg-2 adsorbents, obtained experimentally and calculated using various models: Langmuir (dot line), Freundlich (dash line), Sips (solid line), and Redlich-Peterson (dash-dot line)

Table 3 Calculated parameters of adsorption models for Zr-Ca-Mg and Ti-Ca-Mg phosphates

Models	Parameters	Zr-Ca-Mg-1	Zr-Ca-Mg-2	Ti-Ca-Mg-1	Ti-Ca-Mg-2
	$q_{e,exp}$, mg/g	117.0	37.4	41.5	15.2
Langmuir	q_m, mg/g	120.4	38.11	49.92	16.75
	K_L, L/mg	0.0264	0.0315	0.0044	0.0106
	$\boldsymbol{R^2}$	**0.974**	**0.931**	**0.962**	**0.738**
	SSE	363.3	58.53	49.22	22.91
	SE	7.78	3.42	3.14	2.76
Freundlich	K_F, (mg/g)/(L/mg)^n_F	21.97	10.45	2.37	1.45
	n_F	4.02	5.46	2.39	2.72
	$\boldsymbol{R^2}$	**0.793**	**0.778**	**0.911**	**0.905**
	SSE	2852	187.0	116.0	8.29
	SE	21.81	6.12	4.82	1.66
Sips	q_m, mg/g	112.8	38.74	48.80	20.00
	K_S, L/mg	0.0062	0.0431	0.0047	0.0333
	n_S	1.50	0.90	1.04	0.68
	$\boldsymbol{R^2}$	**0.991**	**0.932**	**0.962**	**0.856**
	SSE	128.7	57.08	49.00	16.08
	SE	5.07	3.78	3.50	2.84
Redlich-Peterson	K_{RP}, L/g	3.18	1.20	0.22	0.75
	a_{RP}, L^g/mg^g	0.0264	0.0315	0.0044	0.2978
	g	1.00	1.00	1.00	0.72
	q_m, mg/g	120.4	38.11	49.92	2.50
	$\boldsymbol{R^2}$	**0.974**	**0.931**	**0.962**	**0.899**
	SSE	363.3	58.53	49.22	11.28
	SE	8.52	3.83	3.51	1.94

The significance of the values ±0.001

For this model, there was also a good correspondence between q_m and $q_{e,exp}$, which allowed using this equation to interpret data and compare the characteristics of adsorbents with each other. Comparing the adsorbents by the K_S parameter, which characterizes the affinity of the adsorbent to adsorbate, it can be seen that in the case of Ti-containing adsorbents, this indicator was lower than for Zr-containing adsorbents. n_S parameter, reflecting the heterogeneity of the surface, confirmed that the samples obtained by treatment with Ti- and Zr-containing solutions with a smaller volume (Zr-Ca-Mg-1 and Ti-Ca-Mg-1) were characterized by greater heterogeneity of phase and chemical composition.

Figure 3 shows the dependence of the removal efficiency of cobalt ions from the solution using composite phosphates depending on the initial concentration of Co(II) ions. Maximum adsorption capacity in the studied range of Co(II) ions concentration varied for composite adsorbents from 17 mg/g for Ti-Ca-Mg-2 phosphate, the least active in the adsorption of Co(II) ions, to 109 mg/g for the Zr-Ca-Mg-1 sample, which was most effective in these processes. According to the adsorption capacity, the studied composite phosphates form a series of Zr-Ca-Mg-1 > Zr-Ca-Mg-2 > Ti-Ca-Mg-1 > Ti-Ca-Mg-2. Herewith, the Zr-Ca-Mg-2 and Ti-Ca-Mg-1 samples were close in terms of the achieved adsorption capacity of cobalt ions.

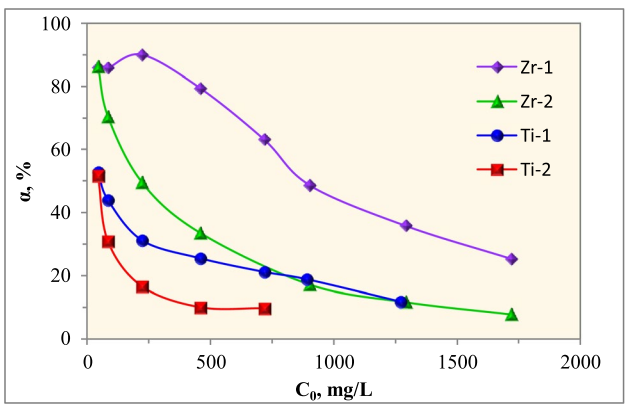

Fig. 3 Effect of initial Co(II) ions concentration on removal efficiency

The maximum adsorption capacity was reached for the Zr-Ca-Mg-1 sample at significantly lower equilibrium concentrations of about 300 mg/L compared to other adsorbents (600 mg/Ll). At the same time, the adsorption isotherm for this sorbent differed from others by the angle of inclination to the ordinate axis, which makes it possible to purify the

solutions more deeply. The removal efficiency of Co(II) ions with an initial concentration of up to 220 mg/L for Zr-Ca-Mg-1 sample was 85–90% (Fig. 3) when for Zr-Ca-Mg-2 adsorbent, it was achieved only for solutions with an initial cobalt concentration of 50 mg/L. The removal efficiency of cobalt ions for Ti-containing composite phosphates did not exceed 50% in the entire studied concentration range.

The shape of the isotherm, on which the initial extended section was located at a small angle to the ordinate axis or almost merges with it (H-type isotherms according to the Giles classification) is characteristic of the so-called heterogeneous exchange reactions occurring at the interface of the phases of the initial sorbent and the reaction product. In this case, based on the composition of Zr-Ca-Mg-1, it can be assumed that calcium and magnesium hydrogen phosphates reacted. Reactions proceed with the formation of less soluble cobalt phosphates. It is important to note that calcium and magnesium hydrogen phosphates are also included in the composition of Ti-Ca-Mg-1 composite phosphate. For these adsorbents, the content of calcium and magnesium hydrogen phosphates was slightly lower than for Zr-Ca-Mg-1, while the capacity of Ti-Ca-Mg-1 was significantly inferior to the capacity of Zr-Ca-Mg-1, which did not correlate with a decrease in the content of calcium and magnesium. This indicated that the higher adsorption capacity was due not only to hydrogen phosphates but also to the amorphous phase. At the same time, amorphous zirconium phosphate was significantly more active in the ion exchange adsorption of cobalt ions than amorphous titanium phosphate.

The chemisorption mechanism of Co(II) ions adsorption was supported by the absence of correlation of the observed sorption characteristics with the textural properties of phosphates. Heterogeneous exchange reactions involving individual calcium and magnesium hydrogen phosphates with cobalt ions, according to our previous studies (Shashkova et al. 2012), proceeded with the formation of medium cobalt phosphate and were described by Eqs. (17, 18). The course of these processes was due to the formation of compounds with less solubility. Amorphous zirconium phosphate, which is part of Zr-Ca-Mg-1, was identical in chemical composition to the crystalline α-$Zr(HPO_4)_2 \cdot H_2O$, whose proton can also be replaced by cobalt ions (Eq. 19).

In this case, the reactions (Eqs. 17–19) should be accompanied by an increase in the pH of the solution. Change of the $pH_{eq.}$ and $pH_{init.}$, depending on Co(II) ions concentration is shown in Fig. 4. The observed changes in pH values did not correlate with the mechanism proposed above. The most intensive adsorption in the region of high concentrations by Zr-containing phosphates was accompanied by acidification of the solution, while in the region of low Co(II) ions concentrations, due to the insignificant release of hydrogen ions, there was no significant decrease in the pH of the equilibrium solution.

For the Ti-Ca-Mg-1 sorbent, the pH practically did not change during Co(II) adsorption. In the case of the Ti-Ca-Mg-2 sample with the lowest adsorption capacity, significant acidification of the solution after sorption was observed in the entire studied concentration range. This was due to the peculiarities of their hydrolytic behavior.

For this purpose, the pH of aqueous solutions after contact with composite phosphates was measured. With daily contact of Zr-Ca-Mg-1 and Ti-Ca-Mg-1 with distilled water with a pH of 6.7, the pH value increased to 7.2, due to protonation of the hydrogen phosphate anion with the formation of hydroxide ions. On the contrary, the suspension pH for Zr-Ca-Mg-2 and Ti-Ca-Mg-2 samples was 6.0 and 5.1, respectively. There was a decrease in pH in comparison with the initial distilled water. Thus, the observed pH values after adsorption were formed as a result of two processes—the

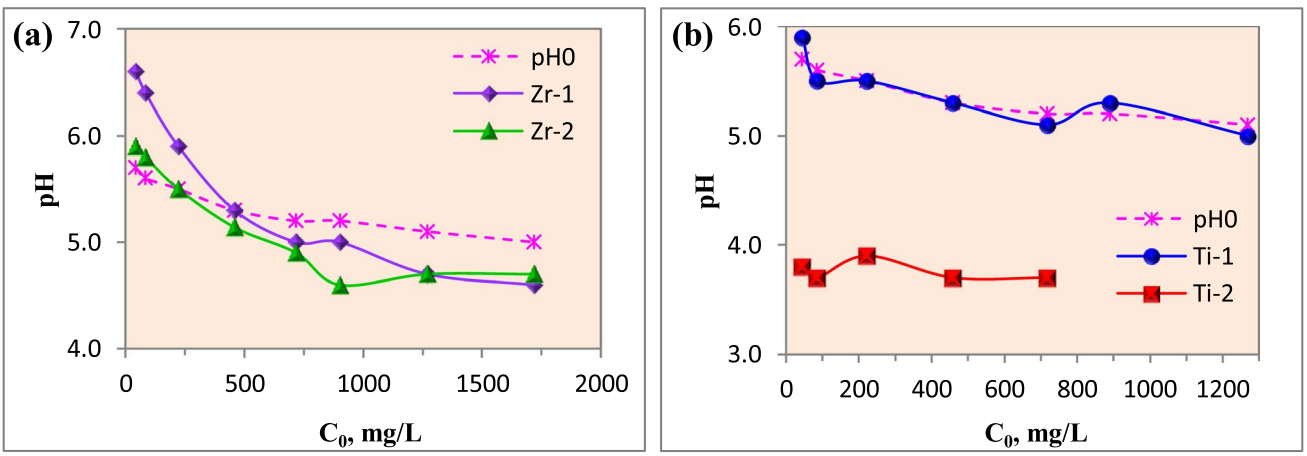

Fig. 4 The dependences of equilibrium solution pH from the initial Co(II) ion concentration before (pH_0) and after adsorption. **a** Zr-Ca-Mg-1 and Zr-Ca-Mg-2. **b** Ti-Ca-Mg-1 and Ti-Ca-Mg-2

hydrolysis of the adsorbent and the ion exchange reaction during Co(II) adsorption.

X-ray diffractograms of adsorbents after Co(II) ions adsorption (Fig. 5) identified reflexes of tertiary cobalt phosphate of varying intensity. For Zr-Ca-Mg-1, which had the largest adsorption capacity, intense peaks of crystalline cobalt phosphate octahydrate $Co_3(PO_4)_2 \cdot 8H_2O$ were observed, as well as less intense reflexes of tertiary phosphate and hydrogen phosphate ions (Fig. 5a).

This indicated that the interaction with Co(II) ions proceeded both by ion-exchange mechanism and because of chemical interaction after the dissolution of the surface layer of the adsorbent and precipitation of cobalt phosphate. The remaining adsorbents after adsorption were a weakly crystallized phase and contained peaks of cobalt phosphate of low intensity or did not contain crystalline phases at all. This was especially for adsorbents containing the largest amount of Zr and Ti ions. At the same time, for Zr-Ca-Mg-2 and Ti-Ca-Mg-1, the capacity of Co(II) ions was at the sensitivity limit of the XRD method (3 wt.%), and for Ti-Ca-Mg-2—beyond it (1.7 wt.%).

Adsorption kinetic studies

The studied composite phosphates also differed in kinetic of Co(II) adsorption (Fig. 6). Up to 50–70% of the Co(II) ions were adsorbed at this concentration in 2 h. The maximum adsorption and output to the plateau were achieved within 4–8 h. For Ti-Ca-Mg-2 and Zr-Ca-Mg-2 samples, adsorption was fast, unlike Ti-Ca-Mg-1 and Zr-Ca-Mg-1 samples, the kinetic curves may indicate the diffusion limitations, access to the unreacted phosphate surface.

Mathematical processing of kinetic curves of Co(II) ions adsorption using pseudo-first and pseudo-second-order equations indicated that the kinetic model of the pseudo-second-order well described ($R^2 > 0.99$) the adsorption kinetics (Table 4).

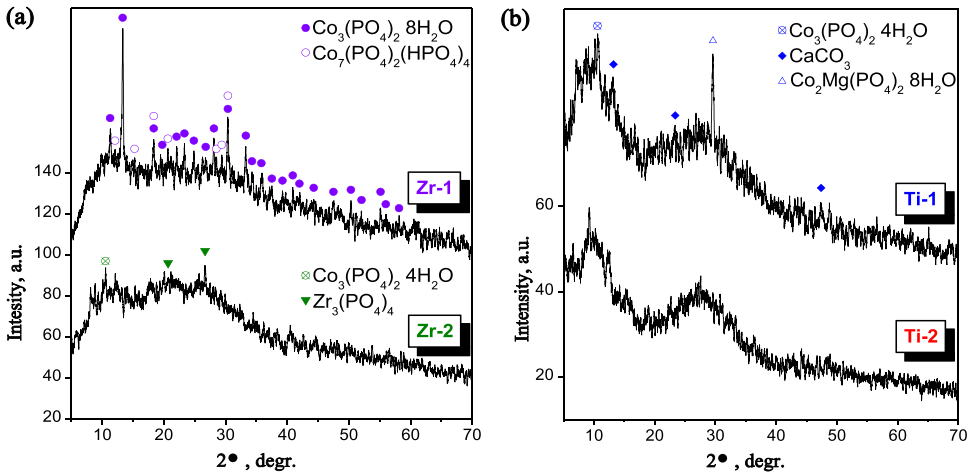

Fig. 5 XRD of **a** Zr-Ca-Mg and **b** Ti-Ca-Mg phosphates after Co(II) ions adsorption

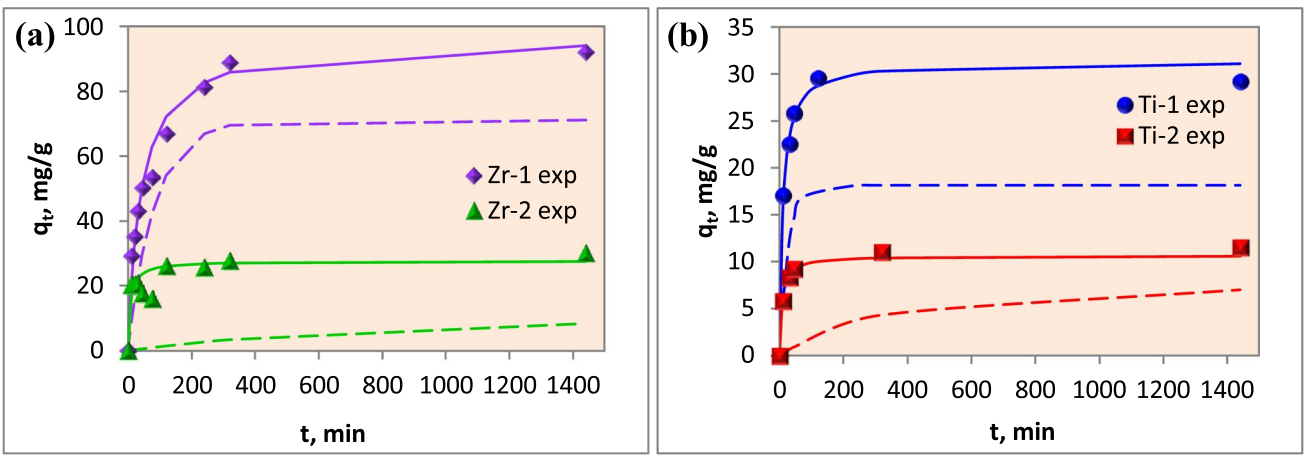

Fig. 6 Experimental kinetic curves of Co(II) ions adsorption by **a** Zr-Ca-Mg and **b** Ti-Ca-Mg phosphates and calculated according to the models of the pseudo-first (dash line) and of a pseudo-second-order (solid line)

Table 4 The calculated parameters of kinetic models for Zr-Ca-Mg and Ti-Ca-Mg phosphates

Samples	q_{exp}, mg/g	Pseudo-first-order			Pseudo-second-order				Intraparticle diffusion		
		q_1, mg/g	$k_1 \cdot 10^3$, 1/min	R^2	q_2, mg/g	$k_2 \cdot 10^3$, g/(mg·min)	h, mg/(g·min)	R^2	k_{id}, mg/(g•min$^{-0.5}$	B_{id}, mg/g	R^2
Zr-1	91.1	71.1	11.91	0.996	96.8	0.25	2.37	0.988	6.08	9.21	0.992
Zr-2	38.5	9.9	1.29	0.750	27.6	4.69	3.58	0.998	0.52	18.44	0.915
Ti-1	29.3	18.1	35.90	0.987	31.3	2.93	2.88	0.991	2.46	9.26	0.999
Ti-2	11.5	7.1	29.04	0.846	10.6	12.50	1.40	0.988	0.97	2.83	0.991

Despite the high values of the approximation coefficients for the pseudo-first-order equation in the case of Ti-Ca-Mg-1 and Zr-Ca-Mg-1 adsorbents, it was more correct to use a pseudo-second-order model, due to the close correspondence of the experimental and theoretically calculated equilibrium capacity (Fig. 7). Comparison of adsorbents by the rate constant k_2 shows that with an increase in the content of Zr and Ti ions in the adsorbents, this parameter increased, especially for a Ti-containing adsorbent.

To determine the limiting stage of the adsorption process, calculations were carried out using the intraparticle diffusion model. As can be seen from the presented data (Table 4, Fig. 7), for the Zr-Ca-Mg-1 and Ti-Ca-Mg-1 adsorbents, the points on the kinetic curve during the initial period of interaction with the solution (30–45 min) had a linear dependence (the correlation coefficient was higher than 0.99, except Zr-Ca-Mg-2 adsorbent). The significant feature of the intra particle diffusion expression is that the linear plots of q_t vs. $t^{0.5}$ should pass through the origin (zero intercept). Thus the intra-particle diffusion model can be easily tested through the above plots provided they have zero intercept, which indicates a controlling influence for the diffusion process on the kinetics. This indicated that the adsorption process at the initial stage was not limited by intraparticle diffusion.

Comparison data

Due to the peculiarities of the state of Co^{2+} ions in solution given in the introduction (Kishi et al., 1998), there is a limited number of adsorbents showing high affinity. The entire spectrum of the studied adsorbents of Co^{2+} ions is presented in reviews (Islam et al. 2018; Joseph et al. 2019). For available low-cost adsorbents based on agricultural and industrial waste or byproducts, the adsorption capacity did not exceed 50 mg/g with a high dose of the adsorbent used—up to 10 g/L. Low capacities were also shown by natural mineral adsorbents (Table 5). Among the enhanced adsorbents, biopolymers and chitosan-containing composites were distinguished, the adsorption properties of which can vary significantly depending on the composition (Vijayaraghavan et al. 2006; Wang et al. 2014; Luo et al. 2018). In some cases, they were even superior to graphene oxide derivatives (Fang et al. 2014). However, it is known that activated carbon substrate is the common prominent adsorbent at their very low dose, its high cost, and difficulty in regeneration. Previously, studies of the sorption properties of Zr-containing materials, including mixed Zr-Ca-Mg phosphates, with respect to Co^{2+} ions have not been conducted. Comparison of the adsorption properties of the obtained adsorbents

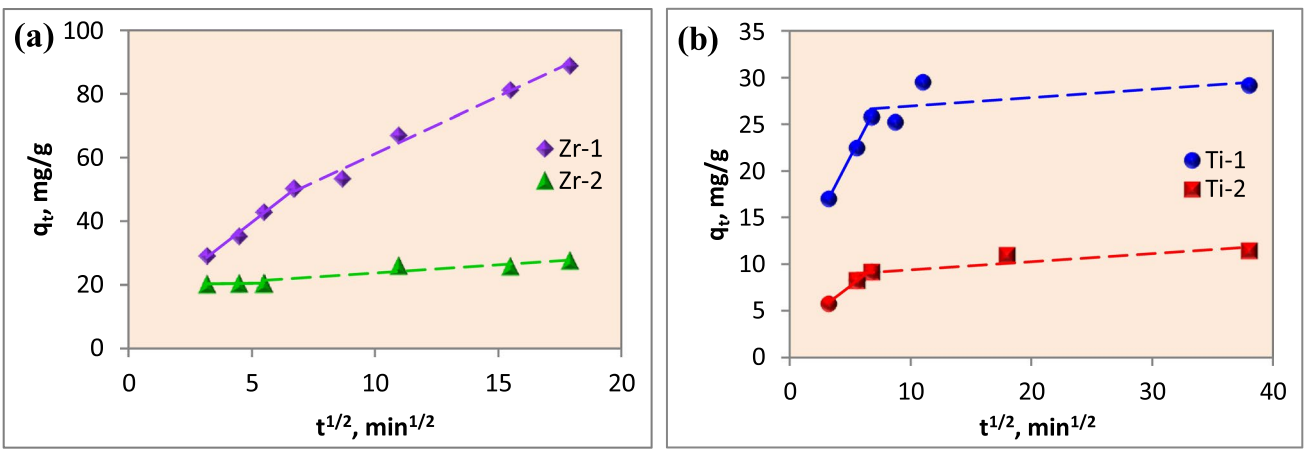

Fig. 7 Kinetic curves of Co(II) ions adsorption by **a** Zr-Ca-Mg and **b** Ti-Ca-Mg phosphates in the coordinates of the intraparticle diffusion model

Table 5 The comparison data for adsorption capacity of prepared Zr-Ca-Mg and Ti-Ca-Mg phosphates

Adsorbent	C_0, mg/L	Dose, g/L	q, mg/g	References
Montmorillonite, natural, and acid-activated	250	2.0	28.6–29.7	Bhattacharyya and Gupta, 2007
Phosphate-modified montmorillonite	1000	20.0	11.8	Ma et al. 2011
Smectite	800–1000	25.0	21.9	Anguile et al. 2013
Amination graphene oxide	1000	0.3	116.4	Fang et al. 2014
Carboxymethyl chitosan beads	20–300	2.0	46.3	Luo et al. 2018
Chitosan–montmorillonite	825	4.0	150	Wang et al. 2014
Crab shell particles	500–2000	5.0	322.6	Vijayaraghavan et al. 2006
Hydroxyapatite	300	5.0	20.9	Smiciklas et al. 2006
Treated animal bones	354	5.0	29.2	Dimovic et al. 2009
TiCaMg-phosphate	1000	5.0	112.0	Maslova et al. 2020
Zr-Ca-Mg-1/2	1000–3000	4.0	156.3–253.3	Present study
Ti-Ca-Mg-1/2	1000–3000	4.0	138.3–212.8	This study

shows the inferior to the best samples of adsorbents and significantly exceeded natural adsorbents, low cost adsorbents, and single-phase calcium phosphates, which emphasizes the advantage of composites.

Conclusions

The facile synthesis from phosphatized dolomite ($Ca_{0.7}Mg_{0.3}HPO_4•2H_2O$) and $ZrO(NO_3)_2$ or $(NH_4)_2TiO(SO_4)_2·H_2O$ aqueous solutions of amorphous Zr-Ca-Mg and Ti-Ca-Mg phosphates with varied Zr (7.8 and 15.1 at.%) and Ti (16.9 and 23.6 at.%) content with mesoporous structure (A_{BET} 19–232 m^2/g, $V_{des.}$ 0.075–0.370 cm^3/g, $D_{des.}$ 6.2–10.9 nm) were performed. The effect of adsorbent chemical composition, the presence of competing ions, and pH of aqueous solution on adsorption removal of Co(II) ions by Zr-Ca-Mg and Ti-Ca-Mg phosphates was studied. Zr-Ca-Mg-1 and Ti-Ca-Mg-1 adsorbents with Zr and Ti content of 7.8 and 16.9 at.% had the highest adsorption capacity of 253.3 and 212.8 mg/g from 0.05 M $Co(NO_3)_2$ solution. The prepared adsorbents demonstrated high efficiency at pH in the range of 3.0–7.0 and the presence of 0.1–1.0 M NaCl and seawater with a salinity of 35.0 g/L backgrounds. The presence of Ca^{2+} competing ions led to a sharply decrease in adsorption capacity of Zr-Ca-Mg-1 and Ti-Ca-Mg-1 samples up to 15.5 and 2.2 mg/g. It was shown that depending on Zr and Ti content in composite Zr-Ca-Mg and Ti-Ca-Mg phosphates, the chemisorption and ion-exchange mechanisms of Co(II) ions removal were revealed. It was supported by well-fitting of adsorption isotherms with Sips and Langmuir models for Zr(Ti)-Ca-Mg-1 and Zr(Ti)-Ca-Mg-2 samples, as well as by well-describing of kinetic data with pseudo-second-order model for prepared adsorbents.

Data availability and materials

Not applicable.

Author contribution Andrei Ivanets: conceptualization, methodology, writing—original; Irina Shashkova: investigation, writing—draft, and results discussion; Natalja Kitikova: investigation, visualization, data curation, data discussion; Natalia Drozdova: investigation, formal analysis; Anastasiya Dzikaya: investigation, formal analysis; Oleg Shichalin: formal analysis, editing; Sofiya Yarusova: formal analysis, editing; Evgeniy Papynov: formal analysis, editing.

Funding This work was financially supported by the National Academy of Sciences of Belarus (Grant No. 21/06–01).

Declarations

Ethics approval We confirm.

Consent to participate Not applicable.

Consent for publication We agree.

Competing interests The authors declare no competing interests.

References

Ali N, Zaman H, Bilal M, Shah AHA, Nazir MS, Iqbal HMN (2019) Environmental perspectives of interfacially active and magnetically recoverable composite materials—a review. Sci Total Environ 670:523–538. https://doi.org/10.1016/j.scitotenv.2019.03.209

Anguile JJ, Mbadcam JK, Ndaghu DD, Dongmo S (2013) Effect of solution parameters on the adsorption of cobalt (II) ions on smectite from Cameroon: equilibrium studies. J Acad Ind Res 2(4):210–215

Balzani P, Kouba A, Tricarico E, Kourantidou M, Haubrock PJ (2021) Metal accumulation in relation to size and body condition in an

all-alien species community. Environ Sci Poll Reshttps://doi.org/10.1007/s11356-021-17621-0
Bhattacharyya KG, Gupta SS (2007) Adsorption of Co(II) from aqueous medium on natural and acid activated kaolinite and montmorillonite. Separ Sci Technol 42(15):339–3418. https://doi.org/10.1080/01496390701515136
Brown PL, Ekberg C (2016) Hydrolysis of metal ions. Wiley-VCH, Verlag GmbH & Co. KGaA, Weinheim, Germany
Cámara-Martos F, Moreno-Rojas R (2016) Cobalt: toxicology. Encycl Food Health. 172–178https://doi.org/10.1016/B978-0-12-384947-2.00176-8
Carolin CF, Kumar PS, Saravanan A, Joshiba GJ, Naushad Mu (2017) Efficient techniques for the removal of toxic heavy metals from aquatic environment: a review. J Environ Chem Eng 5(3):2782–2799. https://doi.org/10.1016/j.jece.2017.05.029
Chen Q, Yao Y, Li X, Lu J, Zhou J, Huang Z (2018) Comparison of heavy metal removals from aqueous solutions by chemical precipitation and characteristics of precipitates. J Water Process Eng 26:289–300. https://doi.org/10.1016/j.jwpe.2018.11.003
Dimovic S, Smiciklas I, Plecas I, Antonovic D, Mitric M (2009) Comparative study of differently treated animal bones for Co^{2+} removal. J Hazard Mater 164:279–287. https://doi.org/10.1016/j.jhazmat.2008.08.013
Dutt MA, Hanif MA, Nadeem F, Bhatti HN (2020) A review of advances in engineered composite materials popular for wastewater treatment. J Environ Chem Eng 8(5):104073. https://doi.org/10.1016/j.jece.2020.104073
Ekka B, Nayak SR, Achary LSK, Sarita KA, Mawatwal S, Dhiman R, Dash P, Patel RK (2018) Synthesis of hydroxyapatite-zirconia nanocomposite through sonochemical route: a potential catalyst for degradation of phenolic compounds. J Environ Chem Eng 6(5):6504–6515. https://doi.org/10.1016/j.jece.2018.09.026
El Batouti M, Al-Harby NF, Elewa MMA (2021) Review on promising membrane technology approaches for heavy metal removal from water and wastewater to solve water crisis. Water 13:3241. https://doi.org/10.3390/w13223241
Fang F, Kong L, Huang J, Wu S, Zhang K, Wang X, Sun B, Zhen J, Wang J, Huang X-J, Liu J (2014) Removal of cobalt ions from aqueous solution by an amination graphene oxide nanocomposite. J Hazard Mater 270:1–10. https://doi.org/10.1016/j.jhazmat.2014.01.031
Ghernaout D, Elboughdiri N (2020) Electrochemical technology for wastewater treatment: dares and trends. Open Access Lib J 7:1–17. https://doi.org/10.4236/oalib.1106020
Hasan HA, Muhammad MH, Ismail NI (2020) A review of biological drinking water treatment technologies for contaminants removal from polluted water resources. J Water Process Eng 33:101035. https://doi.org/10.1016/j.jwpe.2019.101035
Hasan MK, Cheng Y, Kanwar MK, Chu X-Y, Ahammed GJ, Qi Z-Y (2017) Responses of plant proteins to heavy metal stress—a review. Front Plant Sci 8https://doi.org/10.3389/fpls.2017.01492
Islam MA, Morton DW, Johnson BB, Pramanik BK, Mainali B, Angove MJ (2018) Opportunities and constraints of using the innovative adsorbents for the removal of cobalt(II) from wastewater: a review. Environ Nanotechnol Monit Manage 10:435–456. https://doi.org/10.1016/j.enmm.2018.10.003
Ivanets AI, Srivastava V, Kitikova NV, Shashkova IL, Sillanpää M (2017) Non-apatite Ca-Mg phosphate sorbent for removal of toxic metal ions from aqueous solutions. J Environ Chem Eng 5:2010–2017. https://doi.org/10.1016/j.jece.2017.03.041
Ivanets AI, Kitikova NV, Shashkova IL, Roshchina MYu, Srivastava V, Sillanpaa M (2019) Adsorption performance of hydroxyapatite with different crystalline and porous structure towards metal ions in multicomponent solution. J Water Process Eng 32:100963. https://doi.org/10.1016/j.jwpe.2019.100963
Ivanets AI, Shashkova IL, Kitikova NV, Maslova MV, Mudruk NV (2019) New heterogeneous synthesis of mixed Ti-Ca-Mg phosphates as efficient sorbents of ^{137}Cs,^{90}Sr and ^{60}Co radionuclides. J Taiwan Inst Chem Eng 104:151–159. https://doi.org/10.1016/j.jtice.2019.09.001
Ivanets A, Milyutin V, Shashkova I, Kitikova N, Nekrasova N, Radkevich A (2020) Sorption of stable and radioactive Cs(I), Sr(II), Co(II) ions on Ti–Ca–Mg phosphates. J Radioanal Nucl Chem 324:1115–1123. https://doi.org/10.1007/s10967-020-07140-6
Ivanets A, Shashkova I, Kitikova N, Radkevich A, Venhlinskaya E, Dzikaya A, Trukhanov AV, Sillanpaa M (2021) Facile synthesis of calcium magnesium zirconium phosphate adsorbents transformed into $MZr_4P_6O_{24}$ (M: Ca, Mg) ceramic matrix for radionuclides immobilization. Sep Purif Technol 272:118912. https://doi.org/10.1016/j.seppur.2021.118912
Joseph L, Jun B-M, Flora JRV, Park CM, Yoon Y (2019) Removal of heavy metals from water sources in the developing world using low-cost materials: a review. Chemosphere 229:142–159. https://doi.org/10.1016/j.chemosphere.2019.04.198
Khalid S, Shahid M, Niazi NK, Murtaza B, Bibi I, Dumat C (2016) A comparison of technologies for remediation of heavy metal contaminated soils. J Geochem Explor 182:247–268. https://doi.org/10.1016/j.gexplo.2016.11.021
Khan MN, Sarwar A (2007) Determination of points of zero charge of natural and treated adsorbents. Surf Rev Lett 14(03):461–469. https://doi.org/10.1142/s0218625x07009517
Kishi Y, Shigemi S, Doihara S, Mostafa MG, Wase K (1998) Study on the hydrolysis of cobalt ions in aqueous solution. Hydrometall 47:325–338. https://doi.org/10.1016/S0304-386X(97)00056-X
Kobayashi Y, Suzuki H (2013) Cobalt: occurrence, uses and properties. Nova Sci. Publ. Inc., New York
Lima EC, Adebayo MA, Machado FM (2015) Kinetic and equilibrium models of adsorption. In: Bergmann CP, Machado FM (eds) Carbon nanomaterials as adsorbents for environmental and biological applications, Chapter 3. Springer, pp 33–69. https://doi.org/10.1007/978-3-319-18875-1_3
Limousin G, Gaudet J-P, Charlet L, Szenknect S, Barthès V, Krimissa M (2007) Sorption isotherms: a review on physical bases, modeling and measurement. Appl Geochem 22:249–275. https://doi.org/10.1016/j.apgeochem.2006.09.010
Luo W, Bai Z, Zhu Y (2018) Fast removal of Co(II) from aqueous solution using porous carboxymethyl chitosan beads and its adsorption mechanism. RSC Adv 8(24):13370–13387. https://doi.org/10.1039/c7ra13064c
Lyczko N, Nzihou A, Sharrok P (2014) Calcium phosphate sorbent for environmental application. Procedia Eng 83:423–431. https://doi.org/10.1016/j.proeng.2014.09.051
Ma B, Oh S, Shin WS, Choi S-J (2011) Removal of Co^{2+}, Sr^{2+} and Cs^{+} from aqueous solution by phosphate-modified montmorillonite (PMM). Desalin 276:336–346. https://doi.org/10.1016/j.desal.2011.03.072
Maslova M, Mudruk N, Ivanets A, Shashkova I, Kitikova N (2020) A novel sorbent based on Ti-Ca-Mg phosphates: synthesis, characterization, and sorption properties. Environ Sci Pollut Res 27:3933–3949. https://doi.org/10.1007/s11356-019-06949-3
Maslova M, Mudruk N, Ivanets A, Shashkova I, Kitikova N (2021) The effect of pH on removal of toxic metal ions from aqueous solutions using composite sorbent based on Ti-Ca-Mg phosphates. J Water Process Eng 40:101830. https://doi.org/10.1016/j.jwpe.2020.101830
Mohod CV, Dhote J (2013) Review of heavy metals in drinking water and their effect on human health. Int J Innovative Res Sci Eng Technol 2:2992–2996
Mudhoo A, Mohan D, Pittman CU, Sharma G, Sillanpaa M (2021) Adsorbents for real-scale water remediation: gaps and the road

forward. J Environ Chem Eng 9:105380. https://doi.org/10.1016/j.jece.2021.105380

Pan S, Shen J, Deng Z, Zhang X, Pan B (2022) Metastable nano-zirconium phosphate inside gel-type ion exchanger for enhanced removal of heavy metals. J Hazard Mater 423(B):127158. https://doi.org/10.1016/j.jhazmat.2021.127158

Pica M (2021) Treatment of wastewaters with zirconium phosphate based materials: a review on efficient systems for the removal of heavy metal and dye water pollutants. Molecules 26:2392. https://doi.org/10.3390/molecules26082392

Prasad M, Saxena S (2004) Sorption mechanism of some divalent metal ions onto low-cost mineral adsorbent. Ind Eng Chem Res 43(6):1512–1522

Qasem NAA, Mohammed RH, Lawa DU (2021) Removal of heavy metal ions from wastewater: a comprehensive and critical review. Npj Clean Water 4:36. https://doi.org/10.1038/s41545-021-00127-0

Shashkova IL, Rat'ko AL, Drozdova NV (2012) Extraction of Cu^{2+}, Zn^{2+}, and Co^{2+} ions from aqueous solutions with calcium and magnesium phosphates. Russ Appl Chem 85:339–343. https://doi.org/10.1134/S1070427212030020

Singh NB, Nagpal G, Agrawal S, Rachna (2018) Water purification by using adsorbents: a review. Environ Technol Innovation 11:187–240. https://doi.org/10.1016/j.eti.2018.05.006

Smiciklas I, Dimovic S, Plecas I, Mitric M (2006) Removal of Co^{2+} from aqueous solutions by hydroxyapatite. Water Res 40:2267–2274. https://doi.org/10.1016/j.watres.2006.04.031

Vareda JP, Valente AJM, Durães L (2019) Assessment of heavy metal pollution from anthropogenic activities and remediation strategies: a review. J Environ Manage 246:101–118. https://doi.org/10.1016/j.jenvman.2019.05.126

Veliscek-Carolan J, Rawal A, Luca V, Hanley TL (2017) Zirconium phosphonate sorbents with tunable structure and function. Microporous Mesoporous Mater 252:90–104. https://doi.org/10.1016/j.micromeso.2017.05.059

Vijayaraghavan K, Palanivelu K, Velan M (2006) Biosorption of copper(II) and cobalt(II) from aqueous solutions by crab shell particles. Biores Technol 97(12):1411–1419. https://doi.org/10.1016/j.biortech.2005.07.00

Wang J, Guo X (2020) Adsorption isotherm models: classification, physical meaning, application and solving method. Chemosphere 258:127279. https://doi.org/10.1016/j.chemosphere.2020.127279

Wang H, Tang H, Liu Z, Zhang X, Hao Z, Liu Z (2014) Removal of cobalt(II) ion from aqueous solution by chitosan–montmorillonite. J Environ Sci 26(9):1879–1884. https://doi.org/10.1016/j.jes.2014.06.021

Wu F-C, Liu B-L, Wu K-T, Tseng R-L (2010) A new linear form analysis of Redlich-Peterson isotherm equation for the adsorptions of dyes. Chem Eng J 162(1):21–27. https://doi.org/10.1016/j.cej.2010.03.006

Wu Q, Leung JYS, Geng X, Chen S, Huang X, Li H, Huang Z, Zhu L, Chen J, Lu Y (2015) Heavy metal contamination of soil and water in the vicinity of an abandoned e-waste recycling site: implication for dissemination of heavy metals. Sci Total Environ 506–507:217–225. https://doi.org/10.1016/j.scitotenv.2014.10.121

Yarusova SB, Shichalin OO, Belov AA, Azon SA, Buravlev IY, Golub AV, Mayorov VY, Gerasimenko AV, Papynov EK, Ivanets AI, Buravleva AA, Merkulov EB, Nepomnyushchaya VA, Kapustina OV, Gordienko PS (2015) Synthesis of amorphous $KAlSi_3O_8$ for cesium radionuclide immobilization into solid matrices using spark plasma sintering technique. Ceramic Intern 48(3):3808–3817. https://doi.org/10.1016/j.ceramint.2021.10.164

Ziwa G, Crane R, Hudson-Edwards KA (2021) Geochemistry, Mineralogy and microbiology of cobalt in mining-affected environments. Minerals 11:22. https://doi.org/10.3390/min11010022

Terms and Conditions

Springer Nature journal content, brought to you courtesy of Springer Nature Customer Service Center GmbH (“Springer Nature”).
Springer Nature supports a reasonable amount of sharing of research papers by authors, subscribers and authorised users (“Users”), for small-scale personal, non-commercial use provided that all copyright, trade and service marks and other proprietary notices are maintained. By accessing, sharing, receiving or otherwise using the Springer Nature journal content you agree to these terms of use (“Terms”). For these purposes, Springer Nature considers academic use (by researchers and students) to be non-commercial.
These Terms are supplementary and will apply in addition to any applicable website terms and conditions, a relevant site licence or a personal subscription. These Terms will prevail over any conflict or ambiguity with regards to the relevant terms, a site licence or a personal subscription (to the extent of the conflict or ambiguity only). For Creative Commons-licensed articles, the terms of the Creative Commons license used will apply.
We collect and use personal data to provide access to the Springer Nature journal content. We may also use these personal data internally within ResearchGate and Springer Nature and as agreed share it, in an anonymised way, for purposes of tracking, analysis and reporting. We will not otherwise disclose your personal data outside the ResearchGate or the Springer Nature group of companies unless we have your permission as detailed in the Privacy Policy.
While Users may use the Springer Nature journal content for small scale, personal non-commercial use, it is important to note that Users may not:

1. use such content for the purpose of providing other users with access on a regular or large scale basis or as a means to circumvent access control;
2. use such content where to do so would be considered a criminal or statutory offence in any jurisdiction, or gives rise to civil liability, or is otherwise unlawful;
3. falsely or misleadingly imply or suggest endorsement, approval , sponsorship, or association unless explicitly agreed to by Springer Nature in writing;
4. use bots or other automated methods to access the content or redirect messages
5. override any security feature or exclusionary protocol; or
6. share the content in order to create substitute for Springer Nature products or services or a systematic database of Springer Nature journal content.

In line with the restriction against commercial use, Springer Nature does not permit the creation of a product or service that creates revenue, royalties, rent or income from our content or its inclusion as part of a paid for service or for other commercial gain. Springer Nature journal content cannot be used for inter-library loans and librarians may not upload Springer Nature journal content on a large scale into their, or any other, institutional repository.
These terms of use are reviewed regularly and may be amended at any time. Springer Nature is not obligated to publish any information or content on this website and may remove it or features or functionality at our sole discretion, at any time with or without notice. Springer Nature may revoke this licence to you at any time and remove access to any copies of the Springer Nature journal content which have been saved.
To the fullest extent permitted by law, Springer Nature makes no warranties, representations or guarantees to Users, either express or implied with respect to the Springer nature journal content and all parties disclaim and waive any implied warranties or warranties imposed by law, including merchantability or fitness for any particular purpose.
Please note that these rights do not automatically extend to content, data or other material published by Springer Nature that may be licensed from third parties.
If you would like to use or distribute our Springer Nature journal content to a wider audience or on a regular basis or in any other manner not expressly permitted by these Terms, please contact Springer Nature at

onlineservice@springernature.com